10-10-2007

Effect of Surface Roughness on Rate-Dependent Slip in Simple Fluids

Nikolai V. Priezjev
Wright State University - Main Campus, nikolai.priezjev@wright.edu

Effect of surface roughness on rate-dependent slip in simple fluids

Nikolai V. Priezjev*

Department of Mechanical Engineering,

Michigan State University, East Lansing, Michigan 48824

(Dated: October 29, 2018)

Molecular dynamics simulations are used to investigate the influence of molecular-scale surface roughness on the slip behavior in thin liquid films. The slip length increases almost linearly with the shear rate for atomically smooth rigid walls and incommensurate structures of the liquid/solid interface. The thermal fluctuations of the wall atoms lead to an effective surface roughness, which makes the slip length weakly dependent on the shear rate. With increasing the elastic stiffness of the wall, the surface roughness smoothes out and the strong rate dependence is restored again. Both periodically and randomly corrugated rigid surfaces reduce the slip length and its shear rate dependence.

PACS numbers: 68.08.-p, 83.50.Rp, 47.61.-k, 83.10.Rs

I. INTRODUCTION

The description of the fluid flow in confined geometry requires specification of the boundary condition for the fluid velocity at the solid wall. Usually the fluid is assumed to be immobile at the boundary. Although this assumption is successful in describing fluid flow on macroscopic length scales, it needs a revision for the microscopic scales due to possible slip of the fluid relatively to the wall [1]. The existence of liquid slip at the solid surfaces was established in many experiments on the pressure driven flow in narrow capillaries [2, 3, 4] and drainage of thin liquid films in the surface force apparatus [5, 6, 7]. The most popular Navier model relates the fluid slip velocity to the interfacial shear rate by introducing the slip length, which is assumed to be rate-independent. The slip length is defined as a distance from the boundary where the linearly extrapolated fluid velocity profile vanishes. Typical

*http://www.egr.msu.edu/~priezjev

values of the slip length inferred from the experiments on fluids confined between smooth hydrophobic surfaces is of the order of ten nanometers [5, 7, 8, 9, 10]. Despite the large amount of experimental data on the slip length [11], the underlying molecular mechanisms leading to slip are still poorly understood because it is very difficult to resolve the fluid velocity profile in the region near the liquid/solid interface at these length scales.

Over the last twenty years, molecular dynamics (MD) simulations were extensively used to investigate the correlation between the structure of simple fluids in contact with atomically smooth surfaces and slip boundary conditions [12, 13, 14, 15, 16, 17, 18, 19]. The advantage of the MD method is that the fluid velocity profile can be resolved at the molecular level and no assumptions about the slip velocity at the interface are required. The main factors affecting slip for atomically smooth surfaces are the wall-fluid interaction, the degree of commensurability of liquid and solid structures at the interface, and diffusion of fluid molecules near the wall. The slip length was found to correlate inversely with the wall-fluid interaction energy and the amount of structure induced in the first fluid layer by the periodic surface potential [12]. For weak wall-fluid interactions and smooth surfaces, the slip length is proportional to the collective relaxation coefficient of the fluid molecules near the wall [20]. The thermal fluctuations of the wall atoms under the strong harmonic potential reduce the degree of the in-plane fluid ordering and result in larger values of the slip length [12]. On the other hand, an excessive penetration of the wall atoms into the fluid phase reduces the slip velocity for soft thermal walls [21]. Nevertheless, the effect of thermal surface roughness on the slip length in the *shear-rate-dependent* regime was not systematically explored even for atomically smooth walls.

In the original MD study by Thompson and Troian [22] on boundary driven shear flow of simple fluids past atomically smooth rigid walls, the slip length was found to increase nonlinearly with the shear rate for weak wall-fluid interactions. A similar dynamic behavior of the slip length has been reported in thin polymer films [23]. The rate-dependent slip was also observed for the planar Poiseuille flow of simple fluids confined between hydrophobic surfaces with variable size of the wall atoms [24, 25]. The variation of the slip length (from negative to positive values) with increasing shear rate for hydrophilic surfaces [24] can be well described by the power law function proposed in Ref. [22]. In the recent paper [26], we have reported a gradual transition in the shear rate dependence of the slip length, from linear to highly nonlinear function with pronounced upward curvature, by decreasing the

strength of the wall-fluid interaction. Remarkably, in a wide range of shear rates and surface energies, the slip length is well fitted by a power law function of a single variable, which is a combination of the structure factor, contact density, and temperature of the first fluid layer. One of the goals of the present study is to investigate how the rate-dependent slip is affected by the presence of the molecular-scale surface roughness.

Molecular scale simulations of simple [27, 28] and polymeric [29, 30] fluids (as well as recent experiments [31, 32, 33]) have shown that the slip length is reduced in the presence of the surface roughness. The effect is enhanced for smaller wavelengths and larger amplitudes of the surface corrugation [28, 30]. At low shear rates, the reduction of the effective slip length is caused by the local curvature of the fluid flow above macroscopic surface corrugations [28, 34, 35] or by more efficient trapping of the fluid molecules by atomic-scale surface inhomogeneities [12, 14, 27, 28, 36]. The analysis of more complex systems with combined effects of surface roughness and rate dependency poses certain difficulties in the interpretation of the experimental results because the exact dependence of the local slip length on shear rate is often not known.

In this paper, we explore the influence of molecular-scale surface roughness on the slip behavior in a flow of simple fluids driven by a constant force. We will show that the functional form of the rate-dependent slip length is considerably modified by the presence of the thermal, random and periodic surface roughness. The growth of the slip length with increasing shear rate, which is observed for atomically smooth rigid walls, is strongly reduced by periodic and random surface roughness. Soft thermal walls produce very weak rate dependence of the slip length, while the linear behavior is restored for stiffer walls.

The paper is organized as follows. The details of molecular dynamics simulations are described in the next section. Results for the shear rate dependence of the slip length on the thermal and random surface roughness are presented in Section III. The effect of periodic wall roughness on the rate-dependent slip is discussed in Section IV. The summary is given in the last section.

II. MD SIMULATION MODEL

The simulation setup consists of $N = 3456$ fluid molecules confined between two stationary atomistic walls parallel to the xy plane. The molecules interact through the truncated

Lennard-Jones (LJ) potential

$$V_{LJ}(r) = 4\,\varepsilon\left[\left(\frac{\sigma}{r}\right)^{12} - \left(\frac{\sigma}{r}\right)^{6}\right], \tag{1}$$

where ε and σ represent the energy and length scales of the fluid phase with density $\rho = 0.81\,\sigma^{-3}$. The interaction between wall atoms and fluid molecules is also modeled by the LJ potential with the energy $\varepsilon_{\rm wf}$ and length scale $\sigma_{\rm wf}$ measured in units of ε and σ. In all our simulations, wall atoms do not interact with each other and $\sigma_{\rm wf} = \sigma$. The cutoff distance is set to $r_c = 2.5\,\sigma$ for fluid-fluid and wall-fluid interactions.

The steady-state flow was induced by a constant force $\mathrm{f_x}$ in the $\hat{x}$ direction, which acted on each fluid molecule. The heat exchange with external reservoir was controlled by a Langevin thermostat with a random, uncorrelated force and a friction term, which is proportional to the velocity of the fluid molecule. The value of the friction coefficient $\Gamma = 1.0\,\tau^{-1}$ is small enough not to affect significantly the self-diffusion coefficient of the fluid molecules [37, 38]. The Langevin thermostat was applied only along the $\hat{y}$ axis to avoid a bias in the flow direction [12]. The equations of motion for a fluid monomer of mass m are given by

$$m\ddot{x}_i = -\sum_{i\neq j}\frac{\partial V_{ij}}{\partial x_i} + \mathrm{f_x}\,, \tag{2}$$

$$m\ddot{y}_i + m\Gamma\dot{y}_i = -\sum_{i\neq j}\frac{\partial V_{ij}}{\partial y_i} + f_i\,, \tag{3}$$

$$m\ddot{z}_i = -\sum_{i\neq j}\frac{\partial V_{ij}}{\partial z_i}\,, \tag{4}$$

where f_i is a randomly distributed force with $\langle f_i(t)\rangle = 0$ and variance

TABLE I: Root mean-square displacement, $\langle \delta u^2\rangle = 3\,k_BT/\kappa$, divided by the nearest-neighbor distance $d = 0.8\,\sigma$ and the typical oscillation time of the wall atoms tethered about their equilibrium lattice positions as a function of the spring stiffness for $m_w = 4\,m$.

Spring stiffness $\kappa\,[\varepsilon/\sigma^2]$	400	600	800	1200	1600
$\sqrt{\langle\delta u^2\rangle}/d$	0.11	0.09	0.08	0.07	0.06
$2\pi\sqrt{m_w/\kappa}\ [\tau]$	0.63	0.51	0.44	0.36	0.31

$\langle f_i(0) f_j(t)\rangle = 2mk_BT\Gamma\delta(t)\delta_{ij}$ obtained from the fluctuation-dissipation theorem. The temperature of the thermostat is fixed to $T = 1.1\,\varepsilon/k_B$, where k_B is the Boltzmann constant. The equations of motion of the fluid molecules and wall atoms are integrated using the fifth-order gear-predictor method [39] with a time step $\triangle t = 0.002\,\tau$, where $\tau = \sqrt{m\sigma^2/\varepsilon}$ is the LJ time.

The wall atoms were allowed to oscillate about their equilibrium lattice sites under the harmonic potential $V_{sp} = \frac{1}{2}\,\kappa\, r^2$. The spring stiffness κ was chosen so that the ratio of the root mean-square displacement of the wall atoms and their nearest-neighbor distance was less than the Lindemann criterion for melting, $\sqrt{\langle \delta u^2\rangle}/d \lesssim 0.15$, e.g. see Ref. [40]. At the same time, the parameter κ should be small enough so that the dynamics of the wall atoms can be accurately resolved with the MD integration time step. The mass of the wall atoms m_w was chosen to be four times that of the fluid molecule to make their oscillation times comparable. The Langevin thermostat was also applied to all three components of the wall atoms equations of motion, e.g. for the $\hat{x}$ component

$$m_w\,\ddot{x}_i + m_w\,\Gamma\dot{x}_i \;=\; -\sum_{i\neq j}\frac{\partial V_{ij}}{\partial x_i} - \frac{\partial V_{sp}}{\partial x_i} + f_i\,, \tag{5}$$

where the sum is taken over the fluid molecules within the cutoff radius $r_c = 2.5\,\sigma$. Mean displacement of the wall atoms and their typical oscillation time are summarized in Table I for the values of the spring constant considered in this study.

Each wall is constructed out of 648 atoms distributed between two (111) planes of the face-centered cubic (fcc) lattice with density $\rho_w = 2.73\,\sigma^{-3}$. The walls are separated by a distance $24.58\,\sigma$ along the $\hat{z}$ axis. The lateral dimensions of the computational domain in the xy plane are measured as $L_x = 25.03\,\sigma$ and $L_y = 7.22\,\sigma$. Periodic boundary conditions are imposed along the $\hat{x}$ and $\hat{y}$ directions. After an equilibration period of at least $2\times10^4\tau$, the fluid velocity and density profiles were computed for a time interval up to $2\times10^5\tau$ within bins of thickness $\Delta z = 0.2\,\sigma$ and $\Delta z = 0.01\,\sigma$, respectively [26]. The shear viscosity, $\mu = (2.2\pm0.2)\;\varepsilon\tau\sigma^{-3}$, remained independent of the external force [23, 26].

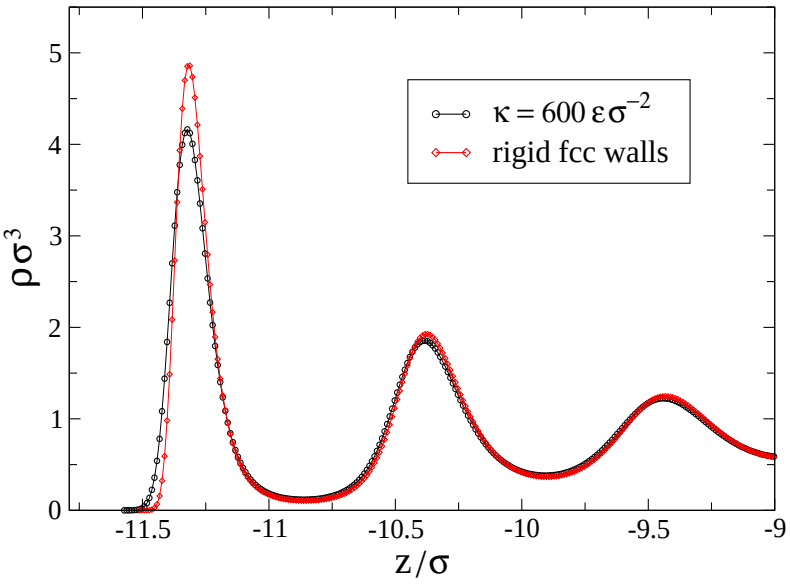

FIG. 1: (Color online) Averaged fluid density profiles near the thermal $\kappa = 600\,\varepsilon/\sigma^2$ ($\circ$) and rigid ($\diamond$) walls for $\varepsilon_{\rm wf}/\varepsilon = 0.9$ and $\mathrm{f_x} = 0.001\,\varepsilon/\sigma$. Left vertical axis coincides with the location of the liquid/solid interface at $z = -11.79\,\sigma$.

III. RESULTS FOR THE THERMAL WALLS

A. Fluid density and velocity profiles

Examples of the averaged fluid density profiles near the thermal and rigid walls are presented in Fig. 1 for a small value of the external force $\mathrm{f_x} = 0.001\,\varepsilon/\sigma$. The first peak in the density profile is slightly broader for the thermal walls because the fluid molecules can move closer to the fcc lattice plane due to finite spring stiffness of the wall atoms. The maximum value of the first peak defines a contact density, which is larger for the rigid walls because of the higher in-plane fluid ordering. In both cases, the fluid density oscillations gradually decay to a uniform bulk profile within $5-6\,\sigma$ away from the wall (not shown). The contact density decreases slightly for larger values of the applied force. A correlation between the fluid structure near the wall and the slip length will be examined in the next section.

The solution of the Navier-Stokes equation for the force driven flow with slip boundary conditions at the confining parallel walls, $\mathrm{v}(\pm h) = V_s$, is given by [1]

$$\mathrm{v}(z) = \frac{\rho\,\mathrm{f_x}}{2\mu}\,(h^2 - z^2) + V_s\,, \tag{6}$$

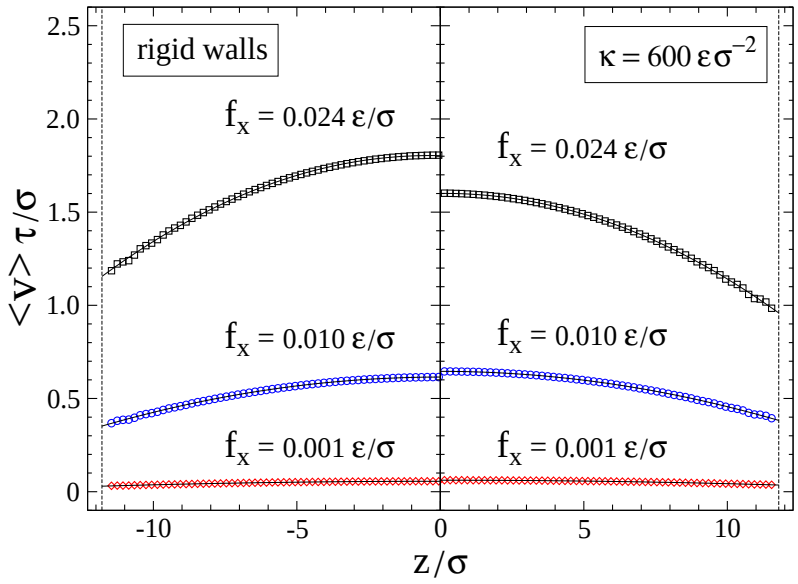

FIG. 2: (Color online) Averaged velocity profiles, $\langle \mathrm{v} \rangle\, \tau/\sigma$, for the indicated values of the applied force per fluid molecule for the rigid walls (left) and the thermal walls with $\kappa = 600\,\varepsilon/\sigma^2$ (right). The wall-fluid interaction energy is fixed to $\varepsilon_{\mathrm{wf}}/\varepsilon = 0.9$. The solid lines represent a parabolic fit to the data. The dashed lines indicate the location of liquid/solid interfaces at $z = \pm\, 11.79\,\sigma$. Vertical axes denote the position of the fcc lattice planes at $z = \pm 12.29\,\sigma$.

where $2h$ is the distance between the walls and μ is the shear rate independent viscosity. The slip length is defined as an extrapolated distance relative to the position of the liquid/solid interface where the tangential component of the fluid velocity vanishes

$$\left| \frac{\partial \mathrm{v}}{\partial z} (\pm h) \right| = \frac{V_s}{L_s} \,. \tag{7}$$

Figure 2 shows representative velocity profiles in steady-state flow for three different values of the external force $\mathrm{f_x}$ and fixed wall-fluid interaction energy $\varepsilon_{\mathrm{wf}}/\varepsilon = 0.9$. The data for thermal and rigid walls are presented only in half of the channel because of the symmetry with respect to the mid-plane of the fluid phase, i.e. $\mathrm{v}(z) = \mathrm{v}(-z)$. Fluid velocity profiles are well fitted by a parabola with a shift by the value of the slip velocity, as expected from the continuum predictions [see Eq. (6)]. The simulation results presented in Fig. 2 show that slip velocity V_s increases with the applied force. The degree of slip depends on the wall stiffness and the interfacial shear rate. The fluid slip velocity is larger for the thermal walls and small forces $\mathrm{f_x} \leqslant 0.012\,\varepsilon/\sigma$. By contrast, rigid walls produce more slippage for the large value of the external force $\mathrm{f_x} = 0.024\,\varepsilon/\sigma$. In both cases, the slip velocity is greater than the

difference between the fluid velocities at the center of the channel and near the walls. The upper bound for the Reynolds number is $Re \approx 10$ [26], ensuring laminar flow conditions throughout.

B. Effect of thermal wall roughness on slip length

Slip boundary conditions for a fluid flow past atomically smooth rigid walls are determined by the molecular-scale surface roughness due to the wall atoms fixed at their equilibrium lattice sites. The thermal fluctuations of the wall atoms, being unavoidable in real surfaces, modify the effective coupling between liquid and solid phases. Depending on the stiffness of the surface, thermal walls can either reduce slip (due to the deep penetration of the wall atoms into the fluid phase) or increase slip because of the reduction of the surface induced structure in the adjacent fluid layer. In this section, the shear rate dependence of the slip length is investigated in a wide range of values of the parameter κ that satisfy the Lindemann criterion for melting (see Table I).

In the previous MD study on shear flow near solids by Thompson and Robbins [12], it was shown that the thermal surface roughness reduces the degree of ordering in the adjacent fluid layer. The thermal fluctuations of the wall atoms produced slip lengths of about $0.5\,\sigma$ larger than their values for the rigid walls. In a wide range of wall-fluid interaction energies $0.2 \leqslant \varepsilon_{\rm wf}/\varepsilon \leqslant 25$, the slip length was found to be rate-independent and less than $3.5\,\sigma$. In our simulations, the surface potential is less corrugated because of the higher wall density; and, therefore, the effect of thermal surface roughness on the slip length is greater.

The variation of the slip length with increasing shear rate for different values of the spring stiffness κ and $\varepsilon_{\rm wf}/\varepsilon = 0.9$ is presented in Fig. 3. The data for smooth rigid walls, fitted by a straight line, are also shown in Fig. 3 for comparison with the results for the thermal walls. In the range of accessible shear rates, the slip length is larger for stiffer thermal walls. The surface becomes effectively smoother because the average displacement of the wall atoms with respect to their equilibrium sites is reduced at larger values of κ. A similar reduction in slip velocity for the soft thermal wall atoms was reported in recent MD simulations of thin films of hexadecane [21]. For soft walls with $\kappa = 400\,\varepsilon/\sigma^2$, the wall atoms penetrate deeper into the fluid phase, which makes the slip length smaller and weakly dependent on the shear rate. For $\kappa = 600\,\varepsilon/\sigma^2$, the slip length increases slightly at low shear rates and

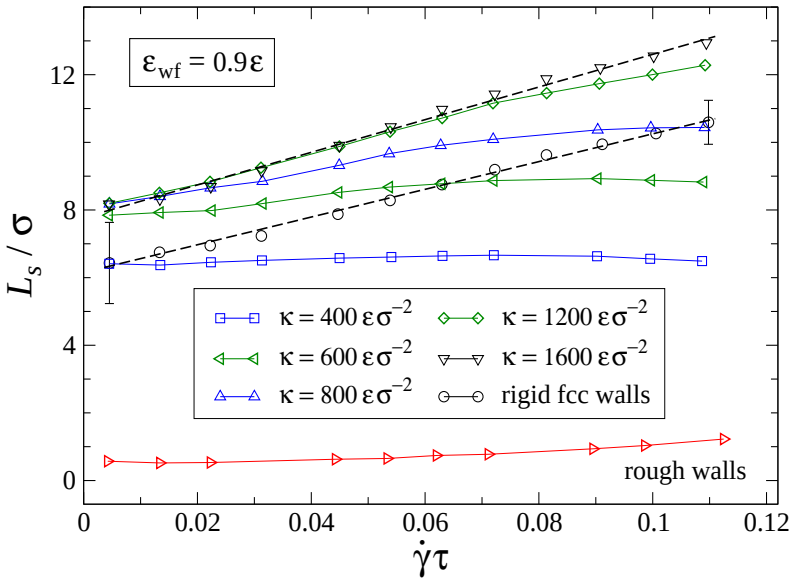

FIG. 3: (Color online) Slip length, L_s/σ, as a function of the shear rate at the interface for $\varepsilon_{\rm wf}/\varepsilon = 0.9$. The values of the spring constant κ for the thermal walls are listed in the inset. The dashed lines represent the best fit to the data for the thermal walls with $\kappa = 1600\,\varepsilon/\sigma^2$ ($\triangledown$) and the rigid fcc walls ($\circ$). The slip length for rough rigid walls with $\langle \delta u^2 \rangle^{1/2} \simeq 0.07\,\sigma$ ($\triangleright$). The solid curves are a guide for the eye.

then saturates at $\dot{\gamma}\tau \gtrsim 0.063$, where it becomes smaller than L_s for the rigid walls. This behavior is consistent with the results for the fluid velocity profiles presented in Fig. 2 for the thermal and rigid walls.

In the case of the largest spring constant $\kappa = 1600\,\varepsilon/\sigma^2$, the slip length increases monotonically with the shear rate and its dependence can also be fitted well by a straight line. The slope of the fitted line is slightly larger than one for the rigid walls (see Fig. 3). For a finite spring stiffness, a small downward curvature appears at $\dot{\gamma}\tau \gtrsim 0.05$ because of the higher temperature and, as a consequence, larger mean displacement of the wall atoms. The maximum increase in temperature of the wall atoms and the adjacent fluid layer is about 10% at the highest shear rates reported in Fig. 3. The fluid temperature at the center of the channel increases up to $1.106\,\varepsilon/k_B$ at the highest $\dot{\gamma}$. The upper bound for the shear rate is determined by the maximum shear stress the liquid/solid interface can support [26]. The simulation results for the thermal walls presented in Fig. 3 demonstrate that the spring stiffness in the model of harmonic oscillators can be an important factor in determining the degree of slip in the rate-dependent regime.

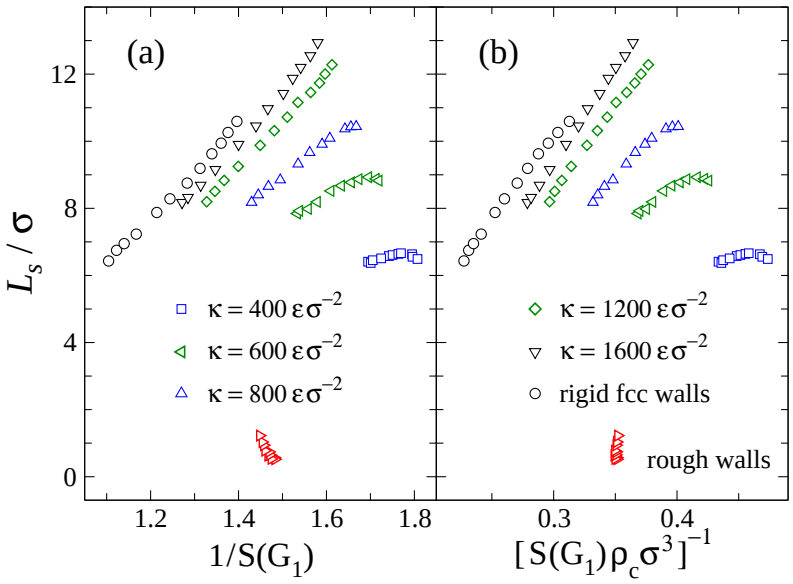

FIG. 4: (Color online) (a) Behavior of the slip length L_s/σ as a function of the inverse value of the in-plane structure factor, $1/S(\mathbf{G}_1)$, evaluated at the first reciprocal lattice vector $\mathbf{G}_1 = (9.04\,\sigma^{-1}, 0)$. The wall-fluid interaction energy is $\varepsilon_{\rm wf}/\varepsilon = 0.9$. (b) The same data for the indicated values of the spring constant are replotted versus $[S(\mathbf{G}_1)\,\rho_c\,\sigma^3]^{-1}$.

It is interesting to note that the surface roughness due to immobile wall atoms with random displacement of only a fraction of a molecular diameter significantly reduces slip length and leads to a slight upward curvature in the rate dependence (see Fig. 3). The rough surfaces were constructed by fixing the instantaneous positions of initially equilibrated wall atoms with the spring stiffness $\kappa = 600\,\varepsilon/\sigma^2$ in the absence of the flow. The parabolic velocity profiles for different values of the applied force were computed for the same realization of disorder. These random perturbations of the surface potential lead to the difference in the slip length of about $7\,\sigma$ in comparison with its values for the thermal walls with the spring stiffness $\kappa = 600\,\varepsilon/\sigma^2$.

The degree of slip at the liquid/solid interface correlates well with the amount of the surface induced order in the adjacent fluid layer [12, 20, 23, 36]. The in-plane fluid structure factor is defined as $S(\mathbf{k}) = 1/N_\ell\ |\sum_j e^{i\,\mathbf{k}\cdot\mathbf{r}_j}|^2$, where $\mathbf{r}_j = (x_j, y_j)$ is the two-dimensional position vector of the j-th molecule and the sum is taken over N_ℓ molecules within the first layer. The effect of periodic surface potential on the structure of the adjacent fluid becomes more pronounced at the reciprocal lattice vectors. In the previous MD study [26] for similar parameters of the wall and fluid phases, it was shown that the slip length scales as

$L_s \sim (\, T_1 / S(\mathbf{G}_1)\, \rho_c)^{\alpha}$, where $\mathbf{G}_1$ is the the first reciprocal lattice vector in the flow direction, T_1 is temperature of the first fluid layer and $\alpha = 1.44 \pm 0.10$. This scaling relation was found to hold in a wide range of shear rates and wall-fluid interactions for atomically smooth rigid walls and incommensurate structures of the liquid/solid interface [26].

The correlation between the inverse value of the fluid structure factor evaluated at the first reciprocal lattice vector $\mathbf{G}_1 = (9.04\,\sigma^{-1}, 0)$ and the slip length is presented in Fig. 4 (a). Except for the rough rigid walls, the surface induced structure in the first fluid layer $S(\mathbf{G}_1)$ is reduced at higher shear rates and smaller values of κ. The slip length increases approximately linearly with $1/S(\mathbf{G}_1)$ for the rigid and stiff walls with $\kappa \geqslant 1200\,\varepsilon/\sigma^2$. A gradual transition to a weak dependence of the slip length on $S(\mathbf{G}_1)$ is observed upon reducing the wall stiffness. In Figure 4 (b) the same data for the slip length are replotted as a function of the inverse product $[S(\mathbf{G}_1)\, \rho_c\, \sigma^3]^{-1}$, where ρ_c is a contact density of the first fluid layer. Although the contact density decreases slightly with increasing the slip velocity, the functional form of the slip length is similar in both cases [see Figs. 4 (a) – 4 (b)]. The results shown in Fig. 4 indicate that the dependence of the slip length on the fluid structure of the first layer is less pronounced for $\kappa \leqslant 800\,\varepsilon/\sigma^2$ due the thermal surface roughness in the rate-dependent regime. Whether the scaling relation for the slip length [26] holds in the presence of the thermal roughness for different wall-fluid interaction energies will be the subject of the future research.

IV. RESULTS FOR PERIODICALLY CORRUGATED WALLS

Next, the results for the rate dependence of the slip length are compared for atomically smooth rigid walls and periodically roughened surfaces. The periodic surface roughness of the upper and the lower walls was modeled by introducing a vertical offset to the positions of the wall atoms $\Delta z(x) = a \sin(2\pi x/\lambda)$ with the wavelength $\lambda = 4.17\,\sigma$. In this part of the study, the wall atoms are rigidly fixed with respect to their equilibrium sites. To properly compare the results for atomically smooth and roughened surfaces, both the local shear rate and the slip length were estimated from a parabolic fit of the velocity profiles at the same location of the interface, i.e. $z = \pm\, 11.79\,\sigma$. A weaker wall-fluid interaction, $\varepsilon_{\rm wf}/\varepsilon = 0.5$, was chosen to obtain larger values of L_s in the absence of the imposed corrugation, since it is expected that the surface roughness strongly reduces the slip length [28].

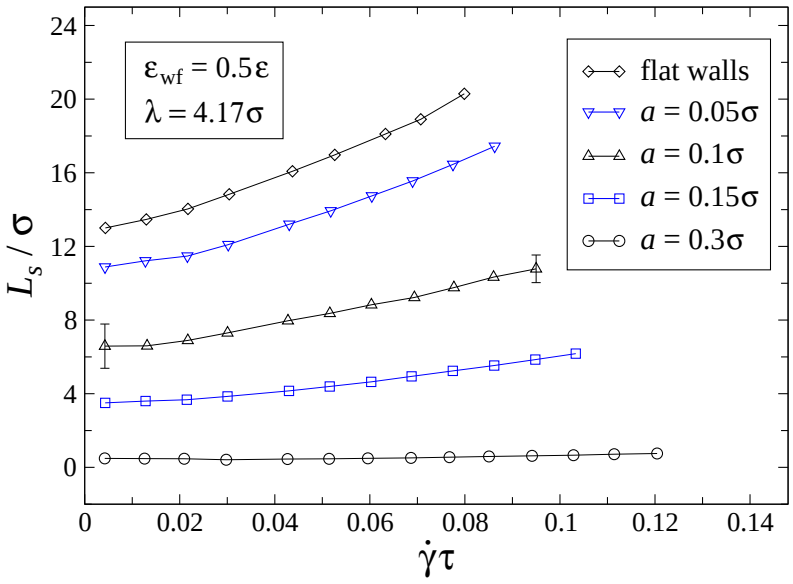

FIG. 5: (Color online) Variation of the slip length L_s/σ as a function of the local shear rate for Poiseuille flows and $\varepsilon_{\rm wf}/\varepsilon = 0.5$. The wavelength and amplitudes of the wall modulation are tabulated in the insets. The local shear rate and the slip length are extracted from a parabolic fit of the velocity profiles at $z = \pm 11.79\,\sigma$.

The dynamic response of the slip length with increasing shear rate is presented in Fig. 5 for atomically smooth and periodically corrugated walls. The data for the flat walls ($a = 0$) are the same as in Ref. [26]. At low shear rates, the slip length L_s° (defined by the leftmost point on each curve in Fig. 5) decreases monotonically with increasing the amplitude a. The no-slip boundary condition is achieved for $a \gtrsim 0.3\,\sigma$. This behavior for a similar geometry and interaction parameters was examined in detail in the previous paper [28]. A direct comparison between continuum analysis and MD simulations showed that there is an excellent agreement between the velocity profiles and the slip length for the large wavelengths $\lambda \gtrsim 20\,\sigma$ and small values of $a/\lambda \lesssim 0.05$. The continuum results overestimate the slip length when λ approaches molecular dimensions [28].

At higher shear rates, the slope of the rate-dependent slip length is gradually reduced with increasing the amplitude of the surface corrugation (see Fig. 5). For the largest amplitude $a = 0.3\,\sigma$, the slip length weakly depends on shear rate and its magnitude becomes smaller than the molecular diameter. As apparent from the set of curves shown in Fig. 5, the same value of the slip length can be obtained by increasing simultaneously the amplitude of the surface corrugation and the shear rate. Analogous behavior of the slip length was observed

experimentally for flows of Newtonian liquids past surfaces with variable nano-roughness [31]. We note, however, that the MD simulations of simple fluids reported in this study do not show any threshold in the rate dependence of the slip length for the amplitudes of the surface corrugation $a \leqslant 0.3\,\sigma$.

V. SUMMARY

In this paper the effect of molecular-scale surface roughness on the slip length in a flow of simple fluids was studied by molecular dynamics simulations. The parabolic fit of the steady-state velocity profiles induced by a constant force was used to define the values of interfacial shear rate and slip length. For atomically smooth rigid surfaces and weak wall-fluid interactions, the slip length increases approximately linearly with the shear rate. Three types of surface roughness were considered: thermal, random and periodic.

The thermal surface roughness due to finite spring stiffness of the wall atoms significantly modifies the slip behavior. The large penetration of the wall atoms into the fluid phase observed for soft walls causes weak rate dependence of the slip length below its values for atomically smooth rigid walls. Increasing the wall stiffness produces effectively smoother surfaces and leads to the linear rate dependence of the slip length. Periodically and randomly corrugated rigid surfaces, with the amplitude below the molecular diameter, strongly reduce the slip length and its shear rate dependence. These findings open perspectives for modeling complex systems with combined effects of surface roughness, wettability and rate dependency.

Acknowledgments

Financial support from the Michigan State University Intramural Research Grants Program is gratefully acknowledged. Computational work in support of this research was performed at Michigan State University's High Performance Computing Facility.

---

[1] G. E. Karniadakis, A. Beskok, and N. Aluru, *Microflows and Nanoflows: Fundamentals and Simulation* (Springer, New York, 2005).

[2] E. Schnell, J. Appl. Phys. **27**, 1149 (1956).

[3] N. V. Churaev, V. D. Sobolev, and A. N. Somov, J. Colloid Interface Sci. **97**, 574 (1984).

[4] C. H. Choi, K. J. A. Westin, and K. S. Breuer, Phys. Fluids **15**, 2897 (2003).

[5] R. G. Horn, O. I. Vinogradova, M. E. Mackay, and N. Phan-Thien, J. Chem. Phys. **112**, 6424 (2000).

[6] J. Baudry, E. Charlaix, A. Tonck, and D. Mazuyer, Langmuir **17**, 5232 (2001).

[7] Y. Zhu and S. Granick, Phys. Rev. Lett. **87**, 096105 (2001).

[8] O. I. Vinogradova and G. E. Yakubov, Phys. Rev. E **73**, 045302(R) (2006).

[9] C. Cottin-Bizonne, B. Cross, A. Steinberger, E. Charlaix, Phys. Rev. Lett. **94**, 056102 (2005).

[10] L. Joly, C. Ybert, and L. Bocquet, Phys. Rev. Lett. **96**, 046101 (2006).

[11] C. Neto, D. R. Evans, E. Bonaccurso, H. J. Butt, and V. S. J. Craig, Rep. Prog. Phys. **68**, 2859 (2005).

[12] P. A. Thompson and M. O. Robbins, Phys. Rev. A **41**, 6830 (1990).

[13] J. Koplik, J. R. Banavar, and J. F. Willemsen, Phys. Fluids A **1**, 781 (1989).

[14] L. Bocquet and J.-L. Barrat, Phys. Rev. E **49**, 3079 (1994).

[15] J.-L. Barrat and L. Bocquet, Phys. Rev. Lett. **82**, 4671 (1999).

[16] K. P. Travis and K. E. Gubbins, J. Chem. Phys. **112**, 1984 (2000).

[17] M. Cieplak, J. Koplik, and J. R. Banavar, Phys. Rev. Lett. **86**, 803 (2001).

[18] V. P. Sokhan, D. Nicholson, and N. Quirke, J. Chem. Phys. **115**, 3878 (2001).

[19] R. Khare, P. Keblinski, and A. Yethiraj, Int. J. Heat Mass Transfer **49**, 3401 (2006).

[20] J.-L. Barrat and L. Bocquet, Faraday Discuss. **112**, 119 (1999).

[21] A. Jabbarzadeh, J. T. Atkinson, and R. I. Tanner, J. Chem. Phys. **110**, 2612 (1999).

[22] P. A. Thompson and S. M. Troian, Nature (London) **389**, 360 (1997).

[23] N. V. Priezjev and S. M. Troian, Phys. Rev. Lett. **92**, 018302 (2004).

[24] S. C. Yang and L. B. Fang, Mol. Simul. **31**, 971 (2005).

[25] S. C. Yang, Microfluidics and Nanofluidics **2**, 501 (2006).

[26] N. V. Priezjev, Phys. Rev. E **75**, 051605 (2007).

[27] T. M. Galea and P. Attard, Langmuir **20**, 3477 (2004).

[28] N. V. Priezjev and S. M. Troian, J. Fluid Mech. **554**, 25 (2006).

[29] J. P. Gao, W. D. Luedtke, and U. Landman, Tribol. Lett. **9**, 3 (2000).

[30] A. Jabbarzadeh, J. T. Atkinson, and R. I. Tanner, Phys. Rev. E **61**, 690 (2000).

[31] Y. Zhu and S. Granick, Phys. Rev. Lett. **88**, 106102 (2002).

[32] T. Schmatko, H. Hervet, and L. Leger, Langmuir **22**, 6843 (2006).

[33] J. Sanchez-Reyes and L. A. Archer, Langmuir, **19**, 3304 (2003).

[34] D. Einzel, P. Panzer, and M. Liu, Phys. Rev. Lett. **64**, 2269 (1990).

[35] S. Richardson, J. Fluid Mech. **59**, 707 (1973).

[36] N. V. Priezjev, A. A. Darhuber, and S. M. Troian, Phys. Rev. E **71**, 041608 (2005).

[37] G. S. Grest and K. Kremer, Phys. Rev. A **33**, 3628 (1986).

[38] M. Tsige and G. S. Grest, J. Chem. Phys. **120**, 2989 (2004).

[39] M. P. Allen and D. J. Tildesley, *Computer Simulation of Liquids* (Clarendon, Oxford, 1987).

[40] J. L. Barrat and J. P. Hansen, *Basic Concepts for Simple and Complex Liquids* (Cambridge University Press, Cambridge, 2003).